

Reply to Reviewer (2)'s comments on gmd-2016-150

We would like to thank the reviewer for careful and thorough reading of this manuscript and for the constructive suggestions. Here are our responses to the reviewer's comments.

Comments to author:

General comments:

The aim of the paper is to introduce a new retrieval cloud method, based on the particle filter approach. Since several very different configuration of cloud can lead to the same observed radiance, PF appears as nice tool for this problem. While similar use of the PF have been introduced in other domains (see comment 1 below), this is a new applications in this fields. The proposed method is compared with state of the art

(MMR) where several particle generating techniques have been considered. The results are well presented with an pedagogical situation to explore the potential of the method, and real cases. The benefit of the PF are a better retrieval at a lower cost compared with the MMR. The manuscript can be improved to facilitate its reading following the comments, and minor revision are required.

Comments:

1) The bibliography on PF focuses on classical data assimilation consideration to estimate initial state. However, PF can also be used to parameter estimation or disaggregation which is similar to what introduced here, see eg Mechri et al. (2015). Hence you should clearly state the difference between the use of PF in classical DA and the present one, even if this relies on the same formalism, and improve the bibliography on this aspect.

Reply: We reorganized the methodology part and added statements as "Particle filter (PF) approach is one of the nonlinear filters for data assimilation procedures to best estimate the initial state of a system or its parameters x_t , which describes the time

evolution of the full probability density function $p(x_i)$ conditioned by the dynamics and the observations. Similar to (Mechri et al., 2014), the bibliography on PF focuses on estimating the parameters, which are the cloud fractions c^k in Eq. (3), in this study.” in paragraph 3 in section 2.

2) Par 1, sec 2, L82: Precise the idea of cloud retrieval: this is implicit but for self consistency it is better to explain (generation of radiance from model, compared with observation, if they match then the cloud structure is found).

Reply: Agreed. More statements are added as “Both cloud retrieval schemes consist of finding cloud fractions that allow best fit between the cloudy radiance from model and the observation.” in the first paragraph in section 2.

3) L87: Precise the level associated with upper script k ($k=1$ means near the surface .. or top atmosphere as encountered in NWP models – Fig. 1 explains it corresponds to the surface, but this should be written) ?

Reply: Accepted. In the revised manuscript, “We use c^1, c^2, \dots, c^K to denote the array of vertical effective cloud fractions for K model levels (c^1 for the surface and c^K for the model top) and c^0 as the fraction of clear sky with $0 \leq c^k \leq 1, \forall k \in [0, K]$.” in section 2.

4) L87: “effective” is not clear, it should be better to explain as the fraction of top of cloud as seen from a sensor.

Reply: Accepted. We revised the statements as “Essentially, the PF cloud retrieval scheme retrieves clouds with the same critical inputs requested (i. e., clear sky radiance from the radiative transfer model and the observed radiance) and the same

cloud retrievals as outputs (i. e., three dimensional cloud fractions, which is defined as the fraction of top of cloud as seen from a sensor) with the MMR method.” in place of effective three dimensional cloud fractions).

5) L88: Following the previous point 4), with the condition $0 \leq c^k \leq 1$, precise that

$$\sum_{k=0}^K c^k = 1$$

at this place, with a label for this equation (the sum can be suppressed from L101).

Reply: Agreed. We labelled the equation and suppressed the sum from L101.

6) L111: the definition of what is a particle is crucial since it use to be model state in classical dynamical system that is not the case here. Hence, you should precise explicitly that P stands for the vector $c = (c^0, c^1, \dots, c^K)$. In the notation, P can be interpreted as a function ck.. I think better to use $C = (c^0, c^1, \dots, c^K)$ for the particle in place of the notation P that could lead to confusion with the probability notation underlined with the particle filter approach. (see point 13 below)

Reply: Accepted. We adopted the reviewer’s idea that using $C = (c^0, c^1, \dots, c^K)$ to interpret the particle, which makes the notations more clear.

7) L113: “typical” provide reference to previous work showing the method is known or suppress “typical”.

Reply: Agreed. We deleted “typical” in the sentence.

8) L115: add an subscript b to c^k in P_b as c_b^k

Reply: Done.

9) L115: “inflating, deflating, moving” should be illustrate using a regular 2D mesh, a simple figure would illustrates the fact that moving can suppress some fraction (a cloud becoming masked by another at upper level).

Reply: Done. The first one is to generate the perturbed samples C_b^i ($\forall i \in [1, n]$) from the cloud profile in the background denoted as $C_b = (c_b^0, c_b^1, \dots, c_b^K)$ by inflating (deflating) the clouds with small magnitudes ($C_b = \alpha \times C_b, \alpha = 50\%, 55\%, \dots, 150\%$) and moving upward (downward) with $\delta z = +5, +4, \dots, -1, \dots, -5$ as the vertical magnitude, where n is the sample size.

10) L111-126: the two approaches (L113) are not clearly separated, make two different paragraph one for each method (L114: the perturbation; L120 L123 the full/fractional one level top cloud)

Reply: Accepted.

11) L126: precise that for one-layer cloud at level i, the clear sky fraction is $c^0 = 1 - c^i$

Reply: Accepted.

12) L130: Eq.(3) means the comparison is done for one frequency.. what happens with other frequency (robustness, sensitivity) ? MMR relies on multiple frequency. At the opposite the PF seems to be used with only one. Please clarify this point / explain

more precisely what is done.

Reply: PF also is conducted based on multiple frequency. We revised the manuscript as “The weight w^i for each particle C_b^i thus is calculated by comparing the simulated $R_{v,i}^{\text{cloud}}$ and the observation R_v^{obs} using the exponential function by accumulating the Jo for multiple frequency as

$$w^i = e^{-\sum_v \left(\frac{R_v^{\text{obs}} - R_{v,i}^{\text{cloud}}}{\sigma} \right)^2}, \quad (5)$$

$\forall i \in [1, p]$.” in sixth paragraph in section 2.

13) L134: with the notation C, Eq.(4) becomes $C_a = \sum_{i=1}^p w^i P_b^i$ which is less confusing than with notation P.

Reply: Accepted.

14) L135: what is mean by updating ? (resampling strategy? analysis step?) I guess you mean analysis step for the particule filter, this should be clarified.

Reply: Corrected. The revised sentence is “After the analysis step for the particle filter, the final averaged cloud fractions...”

15) L135: precise that the average cloud fraction is no more normalised since the constraint (equation labelled from the above comments point 5) is not respected from the average Eq.(4) – average of state is no more a real state.

Reply: Agreed. We added statements as “In Eq. (6), the constraint referred in Eq. (1) is not respected. Thus, after the analysis step for the particle filter, the final averaged cloud fractions C_a^k are normalized by...”

16) L202: Eq.(7) --->Eq.(3)

Reply: Corrected. Since we added two new equations in ahead of Eq. (3), Eq. (3) is labelled as Eq. (5) in the revised manuscript.

17) L203: modify the notation for the prescribed ratio o_f is meaningless (use r, or something else, or explain why this notation is used).

Reply: Agreed.

We re-wrote the sentence as “In Eq. (3), the observation error σ can be set proportional to the observation, equaling to $\frac{R_v^{obs}}{r}$, where r is the prescribed ratio.” in the revised manuscript.

18) L221-224: The particle used there corresponds to the groupe2 described previously, this should be reminded.

Reply: Agreed.

In second paragraph of section 4.1., we added explanations of particles as “To reveal the roles of various initial particles, Fig. 2a shows the weights for different particles of one-layer cloud in group 2 described in section 2 with specified value of cloud fractions (on the x-axis) on specified model levels (on the y-axis) from 10% to 100% every 10% on the given FOV for channel 5 of GOES-Imager for the case shown in Fig. 1.”

19) L224: Detail that the observation can be explained by different possible state and in particular as a fraction c^i of one-cloud layer at a given level i and a fraction of $c^0 = 1 - c^i$ of clear sky since $R_v^{cloud} = c^i R_v^i + (1 - c^i) R_v^0$ for levels i upper than level

5. Hence the theoretical one-layer cloud fraction is the solution of

$$R_v^{obs} = c^i R_v^i + (1 - c^i) R_v^0 \quad \text{that is by } c^i = \frac{R_v^0 - R_v^{obs}}{R_v^0 - R_v^i} .$$

No cloud can be present below level 5 since this would implies an R_v^{cloud} larger then the observation (or a c^i larger than 100%). Provide a representation of the theoretical one-layer fraction so to introduce Fig2. This said, it is then easier to conclude that the weight in Fig2a 2b reproduce these possible situation with a maximum weight concentrated when the fraction is near the theoretical one given above.

Reply: Accepted. We add theoretical representation in the second paragraph in section 4.1 as “With a fraction c^k of one-cloud layer at a given level k and a fraction of $c^0 = 1 - c^k$ of clear sky, the simulated cloudy radiance can be denoted as $R_v^{cloud} = c^k R_v^k + (1 - c^k) R_v^0$. Hence the theoretical one-layer cloud fraction is solved as $c^k = \frac{R_v^0 - R_v^{obs}}{R_v^0 - R_v^k}$ by fitting R_v^{cloud} to R_v^0 . As expected, for one-layer cloud with full fraction, c^5 equals to 100% . Since with the concept that $R_v^k > R_v^{k+1}$, no cloud can be present below level 5 since this would implies a R_v^{cloud} larger than the observation (or a c^i larger than 100%).”

20) L236: What is the normalized Jo ? I guess this should corresponds to the exponent in Eq.(3), but this is not introduced before. Provides the expression of Jo as a function of cloud fraction, it will be easier to understand what represents Fig. 2(c-d), when $C^k = (0, \dots, c^k, 0, \dots, 0)$ with c^k set to 0, 0.1, ... 1 (c) and ... (d)

Reply: Agreed. We add more explanations in section 2 as “A cost function Jo is

defined for each particle to measure how the particle fit the observation as,

$$J_o = \left(\frac{R_v^{\text{obs}} - R_{v,i}^{\text{cloud}}}{\sigma} \right)^2 \quad (4)$$

and also add sentence in section 4.1 as “Here, J_o can be further derived as

$$J_o = r^2 \left(1 - c^0 \frac{R_v^0}{R_v^{\text{obs}}} - c^i \frac{R_v^i}{R_v^{\text{obs}}} \right)^2 \quad (8),$$

with $\sigma = \frac{R_v^{\text{obs}}}{r}$ and $R_v^{\text{cloud}}(c^0, c^1, c^2, \dots, c^K) = c^0 R_v^0 + \sum_{k=1}^K c^k R_v^k$.”

References:

Mechri, R.; Ottele, C.; Pannekoucke, O. Kallel, A. Genetic particle filter application to land surface temperature downscaling Journal Geophysical Research: Atmospheres, 2014, 119, 2131-2146

1 **A method for retrieving clouds with satellite infrared radiances**
2 **using the particle filter**

3 Dongmei Xu^{1,2}, Thomas Auligné², Gaël Descombes², and Chris Synder²

4

5 ¹Key Laboratory of Meteorological Disaster, Ministry of Education (KLME) /Joint
6 International Research Laboratory of Climate and Environment Change (ILCEC)
7 /Collaborative Innovation Center on Forecast and Evaluation of Meteorological
8 Disasters (CIC-FEMD), Nanjing University of Information Science & Technology,
9 Nanjing 210044, China

10

11 ²National Center for Atmospheric Research, Boulder, Colorado 80301, USA

12

12 (2016/8/13)

13

14

anna 2016-07-30 20:16	✓	🗑️
删除的内容: Collaborative Innovation Center on Forecast and Evaluation of Meteorological Disasters, Nanjing University of Information Science & Technology, Nanjing, 210044, China		
anna 2016-08-11 07:21	✓	🗑️
删除的内容: 7		
anna 2016-08-11 07:21	✓	🗑️
删除的内容: 30		

* **Corresponding Author**

Dr. Dongmei Xu

Nanjing University of Information Science & Technology, College of Atmospheric science,

Ningliu road, No. 219, Nanjing, 210044, China

E-mail: xdmjolly@sina.com

15 **Abstract**

16 Ensemble-based techniques have been widely utilized in estimating uncertainties in
17 various problems of interest in geophysical applications. A new cloud retrieval
18 method is proposed based on the efficient Particle Filter (PF) by using ensembles of
19 cloud information in the framework of Gridpoint Statistical Interpolation system
20 (GSI). The PF cloud retrieval method is compared with the Multivariate and
21 Minimum Residual (MMR) method that was previously established and verified.
22 Cloud retrieval experiments involving a variety of cloudy types are conducted with
23 the PF and MMR methods respectively with measurements of Infrared radiances on
24 multi-sensors onboard both geostationary and polar satellites. It is found that the
25 retrieved cloud masks with both methods are consistent with other independent cloud
26 products. MMR is prone to producing ambiguous small-fraction clouds, while PF
27 detects clearer cloud signals, yielding closer heights of cloud top and cloud base to
28 other references. More collections of small fraction particles are able to effectively
29 estimate the semi-transparent high clouds. It is found that radiances with high spectral
30 resolutions contribute to quantitative cloud top and cloud base retrievals. In addition,
31 a different way of resolving the filtering problem over each model grid is tested to
32 better aggregate the weights with all available sensors considered, which is proven to
33 be less constrained by the ordering of sensors. Compared to the MMR method, the PF
34 method is overall more computationally efficient, and the cost of the model grid-based
35 PF method scales more directly with the number of computing nodes.

36 **Keywords:** cloud retrieval methods, particle filter, GSI system, cloud height

37 1. Introduction

38 Modern polar orbiting and geostationary airborne instruments provide researchers
39 unprecedented opportunities for earth remote sensing with continuous flows and
40 almost complete spectral coverage of data. The primary cloud retrieval products from
41 satellites are cloud mask (CM), cloud height (CH), effective cloud fraction (CF), and
42 vertical structures of clouds with larger temporal and spatial scales. These cloud
43 retrievals provide an immense and valuable combination for better initializing
44 hydrometeors in numerical weather prediction (NWP), (Wu and Smith, 1992; Hu et
45 al., 2006; Bayler et al., 2000; Auligné et al., 2011) regulating the radiation budget for
46 the planet, and understanding the climate feedback mechanism (Rossow and Schiffer,
47 1991; Rossow et al., 1993; Brückner et al., 2014). Advanced cloud retrieval methods
48 are able to retrieve clouds with multispectral techniques (Menzel et al., 1983; Platnick
49 et al., 2003), among which the minimization methods usually directly utilize the
50 difference between the modeled clear sky and the observed cloudy Infrared (IR)
51 radiances (e. g., the minimum residual method, (Eyre and Menzel, 1989); the
52 Minimum Local Emissivity Variance method, (Huang et al., 2004); and the
53 Multivariate Minimum Residual method, (Auligné, 2014a)). Specially, the
54 Multivariate Minimum Residual (MMR) method is retrieving three dimensional
55 multi-layer clouds by minimizing a cost function at each field-of-view (FOV)
56 (Auligné, 2014b; Xu et al., 2015). MMR has been proven to be reliable in retrieving
57 the quantitative three dimensional cloud fractions with Infrared radiances from

58 multiple infrared instruments. However, MMR has limitations in several aspects due
59 to its use of minimization for solution: 1) Part of the control variables accounting for
60 the cloud fraction for some certain levels are under-observed since the channels are
61 not sensitive to the existence of clouds for those heights. 2) When clouds at different
62 heights show opacities with the same spectral signal, MMR could lose the ability to
63 distinguish solutions involving clouds at those levels. 3) The computational cost for
64 the minimization procedure in MMR is rather considerable.

65 Ensemble-based techniques, that usually reside in short-term ensemble
66 forecasting (Berrocal et al., 2007), assembling existing model outputs (e. g., cloud
67 retrievals) from varying algorithms (Zhao et al., 2012), or ensemble Kalman filter
68 (EnKF) in various forms (Snyder and Zhang, 2003), have been widely developed in
69 order to estimate the uncertainties of all kinds of problems in geophysical applications.
70 To better account for the non-linearity between the observed radiance and the retrieval
71 parameter, a novel prototype for detecting clouds and retrieving their vertical
72 extension inspired by the particle filter (Snyder and Zhang, 2003; van Leeuwen, 2010;
73 Shen and Tang, 2015) technique and Bayesian theory (Karlsson et al., 2015) is
74 proposed in this study. As a competitive alternative for MMR, the PF retrieval method
75 has same critical inputs required and cloud retrieval products as in MMR. A brief
76 description of MMR and the new PF cloud retrieval algorithm are provided in the
77 following section. Section 3 describes the background model, the data assimilation
78 system, the radiative transfer models (RTMs), and the radiance observations applied
79 in this study. Model configurations are also illustrated in section 3. In section 4, the

80 single test within one FOV is conducted before the performance of PF method is
81 assessed by comparing its cloud retrievals with those from MMR and other
82 operational cloud products. Section 4 also discusses the computational performance
83 for the two methods. The conclusion and anticipated future work are outlined in
84 section 5.

85 2. Methodology

86 Essentially, the PF cloud retrieval scheme retrieves clouds with the same critical
87 inputs requested (i. e., clear sky radiance from the radiative transfer model and the
88 observed radiance) and the same cloud retrievals as outputs (i. e., three dimensional
89 cloud fractions, which is defined as the fraction of top of cloud as seen from a sensor)
90 with the MMR method. Both cloud retrieval schemes consist of finding cloud
91 fractions that allow best fit between the cloudy radiance from model and the
92 observation. We use c^1, c^2, \dots, c^K to denote the array of vertical effective cloud
93 fractions for K model levels (c^1 for the surface and c^K for the model top) and c^0 as
94 the fraction of clear sky with $0 \leq c^k \leq 1, \forall k \in [0, K]$. The constraint for the cloud
95 fraction is as follows,

$$\sum_{k=0}^K c^k = 1$$

97 In this study, a cloud on one model level with a given fraction c^k is assumed to
98 block the radiation from its lower model levels. The radiation originating from its

anna 2016-08-06 19:26 ✓
删除的内容: effective

Administrator 2016-08-11 10:24 ✓
带格式的: 字体颜色: 自动设置

Administrator 2016-08-08 08:35 ✓
删除的内容: Details of the schematic of the MMR method can be referred in (Xu et al., 2015; Descombes et al., 2014).

anna 2016-08-06 20:22 ✓
删除的内容: ,

Administrator 2016-08-11 10:24 ✓
带格式的: 字体颜色: 自动设置

99 lower levels is assumed to contribute to the top of atmosphere radiance observed by
100 the satellites only with the residual fractions.

101 The MMR method is an approach to retrieve cloud fractions using the
102 minimization technique. The residual of the modeled radiance and the observation is
103 normalized by the observed radiance, which results in the following cost function,
104 using $c^k, \forall k \in [0, K]$ as the control variables,

$$105 \quad J(c^0, c^1, c^2, \dots, c^K) = \frac{1}{2} \sum_v \left[\frac{R_v^{\text{cloud}} - R_v^{\text{obs}}}{R_v^{\text{obs}}} \right]^2, \quad (2)$$

106 where R_v^{cloud} is the modeled cloudy radiance, and R_v^{obs} the observed radiance at
107 frequency v . This vertical cloud fraction c^1, c^2, \dots, c^K and c^0 are control variables for
108 the cost function, where the simulated R_v^{cloud} is defined as

$$109 \quad R_v^{\text{cloud}}(c^0, c^1, c^2, \dots, c^K) = c^0 R_v^0 + \sum_{k=1}^K c^k R_v^k. \quad (3)$$

110 Here R_v^k is the radiance calculated assuming an overcast black cloud at the model
111 level k and R_v^0 the radiance calculated in the clear sky. Both R_v^k and R_v^0 are
112 calculated using a forward radiative transfer model with model profiles of temperature
113 and moisture as inputs. Details of the schematic of the MMR method can be referred
114 in (Xu et al., 2015; Descombes et al., 2014).

115 Particle filter (PF) approach is one of the nonlinear filters for data assimilation
116 procedures to best estimate the initial state of a system or its parameters x_i , which
117 describes the time evolution of the full probability density function $p(x_i)$ conditioned
118 by the dynamics and the observations. Similar to (Mechri et al., 2014), the
119 bibliography on PF focuses on estimating the parameters, which are cloud fractions

Administrator 2016-08-10 22:03 ✓

删除的内容: $0 \leq c^k \leq 1, \forall k \in [0, K]$.

anna 2016-08-06 19:54 ✓

删除的内容: 1

anna 2016-08-06 19:54 ✓

删除的内容: 2

anna 2016-08-06 20:00 ✓

删除的内容: with $c^0 + \sum_{k=1}^K c^k = 1$ as the constraint.

120 c^k in Eq. (3), in this study. While MMR retrieves the cloud fractions on each model
121 vertical level by minimizing a cost function, PF calculates posterior weights for each
122 ensemble member based on the observation likelihood given that member. In its
123 simplest form, PF works by initializing a collection of cloud profiles as particles and
124 then estimating the cloud distributions by averaging those particles with their
125 corresponding weights. Explicitly, each particle's weight is computed with the
126 difference between the modeled cloudy radiance from the particle and the observed
127 radiance.

128 As the probabilities of the cloud distribution are fully presented by the initial
129 particles, of particular interest is to evaluate different particle initialization schemes in
130 the PF method. Explicitly, the definition of particles corresponds with ensemble
131 members, i.e. one cloud profile as one of particles is corresponding to an ensemble
132 member.

133 Two approaches for generating particles are firstly designed; the first one is to
134 generate the perturbed samples C_b^i ($\forall i \in [1, n]$) from the cloud profile in the
135 background denoted as $C_b = (c_b^0, c_b^1, \dots, c_b^K)$ by inflating (deflating) the clouds with
136 small magnitudes ($C_b = \alpha \times C_b, \alpha = 50\%, 55\%, \dots, 150\%$) and moving upward
137 (downward) with $\Delta z = +5, +4, \dots, -1, \dots, -5$ as the vertical magnitude, where n is the
138 sample size. The perturbed cloud fractions are designated to replenish the ensemble
139 by introducing the prior information of the cloud distributions from the background
140 and to increase the ensemble spread.

anna 2016-08-06 09:43	✓	🗑️
删除的内容: typical		
anna 2016-07-30 20:22	✓	🗑️
删除的内容: $P_b(\mathbf{c} = c^0, c^1, \dots, c^K)$		
Administrator 2016-08-08 12:54	✓	🗑️
删除的内容: ,		
Administrator 2016-08-08 12:54	✓	🗑️
删除的内容: , and moving		

141 Besides those perturbed particles, to represent the existence of one-layer cloud
 142 on each model level with an even chance, another diversity set of profiles C_b^i
 143 ($\forall i \in [0, K]$) are also initialized, among which, C_b^i stands for the profile with 100%
 144 cloud fraction on the model level i ($c^i=100\%$) and 0% cloud on the rest levels. In
 145 particular, C_b^0 defines 100% clear ($c^0=1$). It is also interesting to discretize the initial
 146 particles by setting the one-layer cloud with the value of c^i from 100% to 0% (e. g.,
 147 100%, 90%, 80%, ..., 0% with 10% as the interval) and further from 100% to 0% (e.
 148 g., 100%, 99%, 98%, 97%, ..., 0% with 1% as the interval). In this cases, $c^0=1-c^i$. For
 149 each particle C_b^i , its simulated cloudy radiance $R_{v,i}^{\text{cloud}}$ from the model background can
 150 be obtained with Eq. (2).

151 A cost function J_o is defined for each particle to measure how the particle fit the
 152 observation as,

$$153 J_o = \left(\frac{R_v^{\text{obs}} - R_{v,i}^{\text{cloud}}}{\sigma} \right)^2. \quad (4)$$

154 The weight w^i for each particle C_b^i thus is calculated by comparing the simulated
 155 $R_{v,i}^{\text{cloud}}$ and the observation R_v^{obs} using the exponential function by accumulating the
 156 J_o for multiple frequency as

$$157 w^i = e^{-\sum_v \left(\frac{R_v^{\text{obs}} - R_{v,i}^{\text{cloud}}}{\sigma} \right)^2}, \quad (5)$$

158 $\forall i \in [1, p]$. Here p is the particle size and σ is the specified observation error, which
 159 can be referred in the first paragraph in section 4.1. The final analyzed C_a is obtained
 160 by averaging the background particles C_b^i with their corresponding weight, as

anna 2016-07-30 20:25 ✓

删除的内容: P_b

anna 2016-07-30 20:26 ✓

删除的内容: Pⁱ

anna 2016-07-30 20:26 ✓

删除的内容: P⁰

anna 2016-07-30 20:26 ✓

删除的内容: P_b

anna 2016-08-06 19:17 ✓

带格式的: 缩进: 首行缩进: 0 字符

anna 2016-07-30 20:26 ✓

删除的内容: P_b

anna 2016-08-06 19:15 ✓

带格式的: 字体: 倾斜

anna 2016-08-06 19:14 ✓

带格式的: 下标

anna 2016-08-06 19:55 ✓

删除的内容: 3

anna 2016-08-06 19:15 ✓

删除的内容:

Administrator 2016-08-10 22:10 ✓

删除的内容: P

anna 2016-07-30 20:28 ✓

删除的内容: P_b

161

$$C_a = \sum_{i=1}^p w^i C_b^i. \quad (6)$$

162

In Eq. (6), the constraint referred in Eq. (1) is not respected. Thus, after the analysis

163

step for the particle filter, the final averaged cloud fractions C_a^k are normalized by

164

$$c_a^k = \frac{c^k}{\sum_{k=0}^K c^k}, \quad (7)$$

165

where $\forall k \in [0, K]$.

166

3. Data and model configurations

167

3.1 Data

168

The Advanced Infrared Sounder (AIRS), the Infrared Atmospheric Sounding

169

Interferometer (IASI), and the Cross-track Infrared Sounder (CrIs) are among the

170

most advanced hyperspectral infrared sounders and thus are applied for retrieving

171

clouds with hundreds of channels (Blumstein et al., 2004) (Aumann et al., 2003; Xu

172

et al., 2013; Smith et al., 2015). The Radiance measurements from Moderate

173

Resolution Imaging Spectroradiometer (MODIS) onboard the Earth Observing

174

System (EOS) Terra or Aqua satellites are also well suited to extracting valuable

175

cloud information from the 36 spectral broadbands in the visible, near infrared and

176

infrared regions at high spatial resolution (1–5 km) (Ackerman, 1998). Apart from

177

the IR radiances from polar satellites, the Geostationary Operational Environmental

178

Satellites (GOES) Imager (Menzel and Purdom, 1994) provides a continuous stream

anna 2016-08-06 19:55	✓	🗑️
删除的内容: 4		
Administrator 2016-08-07 18:23	✓	🗑️
删除的内容: A		
anna 2016-08-06 10:23	✓	🗑️
删除的内容: updating all the particles		
anna 2016-08-06 11:17	✓	🗑️
带格式的: 右		
anna 2016-08-06 11:17	✓	🗑️
删除的内容:		
anna 2016-08-06 11:17	✓	🗑️
删除的内容:		
anna 2016-08-06 19:55	✓	🗑️
删除的内容: 5		

Administrator 2016-08-10 23:06	✓	🗑️
删除的内容: (
Administrator 2016-08-10 23:06	✓	🗑️
删除的内容:)		
Administrator 2016-08-10 23:06	✓	🗑️
删除的内容: (

179 of data over the observing domain. In this study, GOES-13 (east) and GOES-15
180 (west) are [also](#) utilized to obtain cloud fractions over the continental United States
181 (CONUS) domain. The GOES Imager used in this study is a five-channel (one
182 visible, four infrared) imaging radiometer designed to sense radiant and solar
183 reflected energy. The instrument parameters for the sensors and the setups for
184 channel selections can be found in (Xu et al., 2015).

185 3.2 WRF, GSI and the radiative transfer model

186 The background fields are processed running the Weather Research and Forecast
187 (WRF) model (Skamarock et al., 2008). The MMR and PF cloud retrieval algorithms
188 are both implemented based on the gridpoint statistical interpolation data assimilation
189 system (GSI) ([Wu et al., 2002](#); [Kleist et al., 2009](#)), which is a widely used data
190 assimilation system in operations and researches in NWP. GSI is capable of ingesting
191 a large variety of satellite radiance observations and has developed capabilities for
192 data thinning, quality control, and satellite radiance bias correction. The Community
193 Radiative Transfer Model ([Liu and Weng, 2006](#); [Han et al., 2006](#)) was used as the
194 radiance forward operator for computing the clear-sky radiance and the radiance given
195 overcast clouds at each model level.

196 3.3 Model configurations

197 The WRF is configured with 415*325 horizontal grids at 15-km grid spacing, and
198 40 vertical levels up to 50 hPa within the single CONUS domain. The MMR and PF

Administrator 2016-08-10 22:59 ✓ ⌵
删除的内容: (
Administrator 2016-08-10 23:00 ✓ ⌵
删除的内容: (!!! INVALID CITATION !!!)

Administrator 2016-08-10 23:00 ✓ ⌵
删除的内容: (
Administrator 2016-08-10 23:00 ✓ ⌵
删除的内容: (!!! INVALID CITATION !!!)

199 cloud detection schemes search the cloud top using approximately 150 hPa as the
200 highest extent for most cloudy cases. Other clouds higher 150 hPa, e.g. an anvil cloud
201 in a mature thunderstorm around tropopause at low latitude region will also be
202 explored in future studies. Channels in the longwave region are utilized following the
203 channel selection scheme in (Xu et al., 2015). Since the final retrieval clouds are on
204 model grids, the retrieved cloud fractions within one FOV are essentially extrapolated
205 to its four neighboring model grid points. Generally, for each FOV, the retrieved
206 cloud fractions are extrapolated to its four neighboring model grid points. For polar
207 satellite pixels, the representative cloud fractions are extrapolated with an adaptive
208 radius with respect to their scan positions. The cloud detecting procedure for
209 retrieving clouds is conducted for each FOV from each individual sensor
210 independently and sequentially. Since the clouds are retrieved FOV by FOV and the
211 clouds on grids are referred immediately after one FOV is completed, there is no
212 obvious accuracy loss of radiance observations using this conservative method.

Administrator 2016-08-11 10:28 ✓
带格式的: 字体颜色: 自动设置

213 4. Experiments and results

214 The PF experiments apply two groups of particles as mentioned in section 2,
215 among which the group-2 particles contains solely 100% one-layer clouds. To reveal
216 how the setup of the initial particles impacts the results, apart from the MMR and PF
217 experiments, we included another advanced experiment, denoted as APF. APF
218 requires more sampled particles including ranges of cloud fractions spanning from 0%
219 to 100% at the interval of 10%. An additional experiment “APFg2”, similar to APF

220 but excluding the perturbed particles from the background in group-1 introduced in
221 section 2, was conducted to evaluate the added values from the group-one particles. In
222 this section, cloud retrieval experiments for several cases containing clouds of a
223 variety of types are conducted for comparison reason. The GOES imager retrieved
224 products from National Aeronautics and Space Administration (NASA-Langley cloud
225 and radiation products) are applied as a reference to validate the cloud retrieving
226 methods for the CONUS domain with a large and uniform coverage of cloud mask. In
227 addition, the retrieved cloud products were also compared to available CloudSat
228 (Stephens et al., 2002) and MODIS level-2 cloud products (Platnick et al., 2003)
229 archived by the CloudSat Data Processing Center in Colorado State and NASA
230 respectively.

231 4.1 Single test at one field of view

232 The PF cloud retrieving algorithm retrieves the cloud distributions by averaging
233 those initial particles with their weights. Before the real case experiments are carried
234 out over the whole domain, we conduct a single cloud retrieving test at one FOV to
235 understand what differences can be explained by the differences in the basic initial
236 particles. In Eq. (5), the observation error σ can be set proportional to the

237 observation, equaling to $\frac{R_v^{\text{obs}}}{r}$, where r is the prescribed ratio. Thus, the cloud

238 signals on each level k are virtually determined by the extent of how close the $\frac{R_v^k}{R_v^{\text{obs}}}$

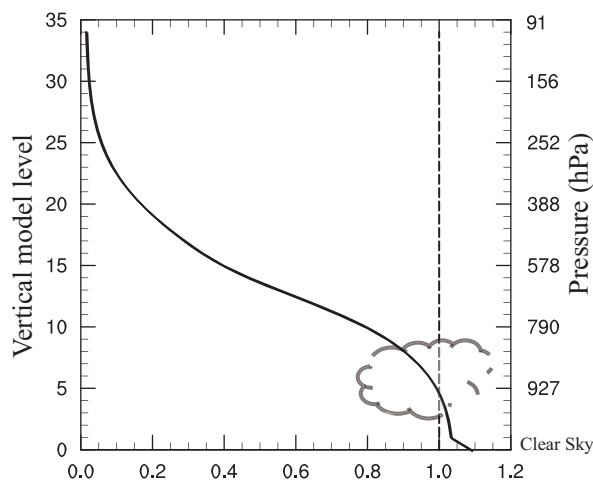
239 (and $\frac{R_v^0}{R_v^{\text{obs}}}$ for the clear part) gets to 1. An example of the ratio of the overcast

anna 2016-08-06 19:55 ✓

删除的内容: 7

240 radiance and the observed radiance $\frac{R_v^k}{R_v^{obs}}$ for each model level is given in Fig. 1 of
 241 GOES-Imager for the channel 5 ($\sim 13.00 \mu m$). The clear sky radiance normalized by
 242 the observed radiance $\frac{R_v^0}{R_v^{obs}}$ is also shown at the level 0 (Fig. 1). It is expected that
 243 the overcast radiance from the RTM decrease with the rising of the altitude. The cloud
 244 signal is strongest around level 5, where R_v^k fits R_v^{obs} most closely. The cloud
 245 retrievals depend not only on the basic input profiles (i.e., the overcast radiance on
 246 each level from RTM normalized by the observed radiance and the clear sky radiance
 247 from RTM normalized by the observed radiance) and but also on the algorithm
 248 applied for resolving the problem (e.g., MMR and PF in this study).

249



250

251 **Figure 1.** Ratio of the overcast radiances versus the observed radiance starting from the level 1.
 252 The ratio of the clear sky radiance normalized by the observed radiance corresponds to the level 0
 253 (see text for explanation) for GOES-Imager for the channel 5. The approximate pressures
 254 corresponding to the model levels are also denoted.

255 To reveal the roles of various initial particles, Fig. 2a shows the weights for
 256 different particles of one-layer cloud in group 2 described in section 2 with specified
 257 value of cloud fractions c^k (on the x-axis) on specified model levels k (on the y-axis)
 258 from 10% to 100% every 10% on the given FOV for channel 5 of GOES-Imager for
 259 the case shown in Fig. 1. With a fraction c^k of one-cloud layer at a given level k and
 260 a fraction of $c^0 = 1 - c^k$ of clear sky, the simulated cloudy radiance can be denoted as
 261 $R_v^{\text{cloud}} = c^k R_v^k + (1 - c^k) R_v^0$. Hence the theoretical one-layer cloud fraction is solved as
 262 $c^k = \frac{R_v^0 - R_v^{\text{obs}}}{R_v^0 - R_v^k}$ by fitting R_v^{cloud} to R_v^0 . As expected, for one-layer cloud with full
 263 fraction, c^5 fits most closely to 100%. Since with the concept that $R_v^k > R_v^{k+1}$, no
 264 cloud can be present below level 5 since this would implies a R_v^{cloud} larger than the
 265 observation (or a c^i larger than 100%). It seems that clouds can be described by
 266 different possible states as particles with both large fractions and small fractions. Low
 267 clouds are easily estimated by one-layer cloud profile with large fractions (larger than
 268 10%). The particles with small-fraction high clouds gain some weights to retrieve
 269 high clouds. The particle with the one-layer cloud on level 13 seems to gain least
 270 weight compared to the others levels. The weights for the particles with cloud
 271 fractions from 0% to 100% at the interval of 1% are also presented in Fig. 2b. By
 272 including more small-fraction one-layer clouds, the clouds around level 13 can be
 273 reproduced by the group of refined particles with 1% as the interval for approximate
 274 10% cloud fractions. However, changing the level of the cloud for the fixed fraction
 275 (10%) does not seem to change the outgoing radiance much, probably due to the
 276 channel's low weight function peak (~750hPa).

Administrator 2016-08-08 11:06 ✓ 
 带格式的: 字体: 倾斜

Administrator 2016-08-11 10:35 ✓ 
 带格式的: 字体颜色: 自动设置

Administrator 2016-08-11 10:35 ✓ 
 带格式的: 字体颜色: 自动设置

Administrator 2016-08-11 10:35 ✓ 
 带格式的: 字体颜色: 自动设置

Administrator 2016-08-08 11:13 ✓ 
 删除的内容: by

277 The normalized J_o in Eq. (6) for different levels with a specific cloud fraction
 278 from 0% to 100% every 10% are shown in the bottom panel of Fig. 2, with 10% and
 279 1% as the intervals in Fig. 2c and Fig. 2d respectively. Here, J_o can be further derived
 280 as

$$281 \quad J_o = r^2 \left(1 - c^0 \frac{R_v^0}{R_v^{obs}} - c^k \frac{R_v^k}{R_v^{obs}} \right)^2 \quad (8).$$

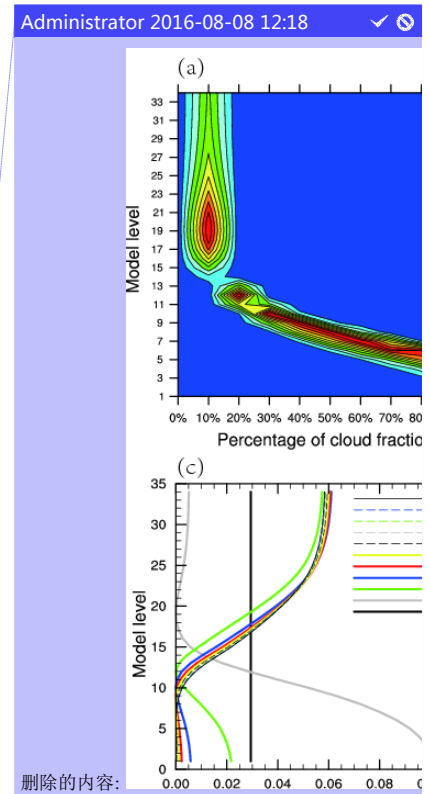
282 with $\sigma = \frac{R_v^{obs}}{r}$ and $R_v^{cloud}(c^0, c^1, c^2, \dots, c^K) = c^0 R_v^0 + \sum_{k=1}^K c^k R_v^k$.

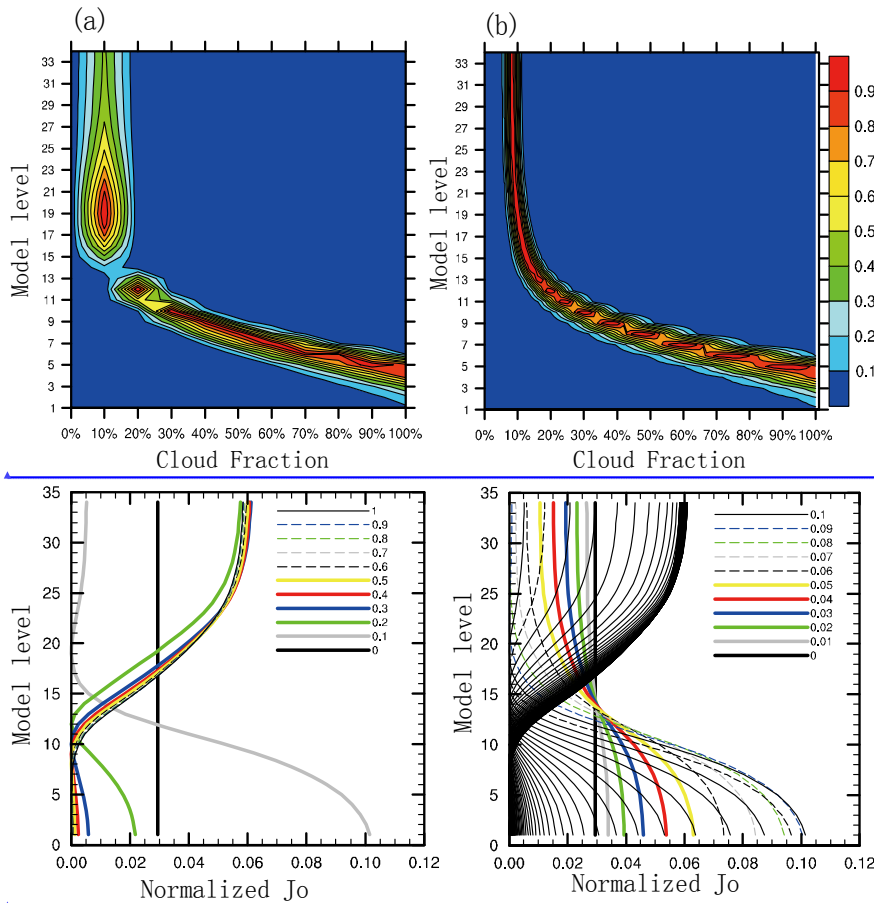
283 From Fig. 2c, it is found that J_o is smallest around level-5 with 100% cloud
 284 fraction (denoted as 1 in legend) for the thin black line, with respect to the fact that
 285 the overcast radiance fits the observed radiance most closely for level-5
 286 approximately. The gray line with 10% cloud fraction (0.1 in the legend) corresponds
 287 to the existence of a weight peak on level 19 in Fig. 2a. In addition, the gap between
 288 the gray line with 0.1 and the other lines from 0.2 to 1 explains why there's less
 289 continuity around level 13. Fig. 2d shows a similar pattern to Fig. 2c, except with
 290 densely-distributed J_o values around the level 13 from 0.1 to 1 in the legend. Those
 291 contiguous black lines in Fig. 2d are associated with the set of particles with cloud
 292 fractions from 10% to 100% at the interval of 1%.

293

294

Administrator 2016-08-11 13:50 ✓
 删除的内容:





Administrator 2016-08-08 12:18 ✓

带格式的: 字体: 加粗

Administrator 2016-08-08 12:19 ✓

带格式的: 字体: 加粗

295

296

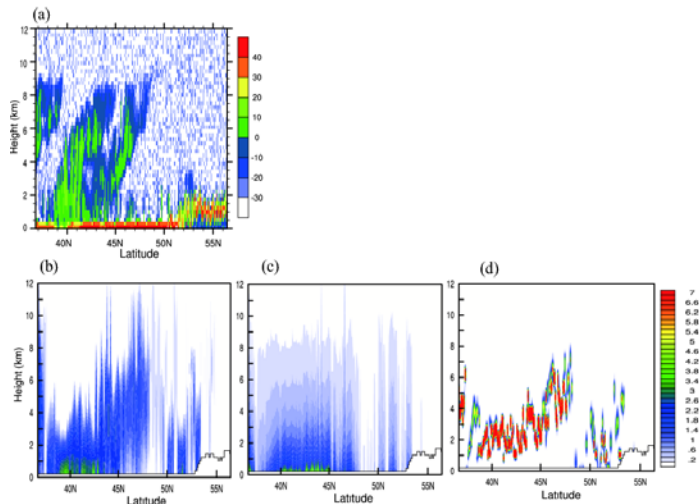
297 **Figure 2.** The weights for different particles with specified cloud fractions on the x-axis at one
 298 chosen model level shown on the y-axis from 0% to 100% (a) at the interval of 10% and (b) at the
 299 interval of 1%. The normalized J_o (c) at the interval of 10% and (d) at the interval of 1%. In (d),
 300 the normalized J_o from 0.1 to 1 are all denoted as black lines.

301 4.2 Cloud profiles

302 The retrieval experiments for a real case are conducted at 1100 UTC 3 June 2012
 303 when AIRS measurements and the CloudSat “2B-GEOPROF” products (Mace, 2004)

304 are available. The vertical cross sections of the cloud fraction field of a real case are
305 illustrated to further check how different collections of initial particles impact the
306 retrieved cloud profiles. The standard radar reflectivity profiles from the CloudSat are
307 shown in Fig. 3a as the validation source; Fig. 3b, Fig. 3c, and Fig. 3d show the cross
308 sections of the cloud fractions along the CloudSat orbit tracks from the MMR, PF and
309 APF experiments. The vertical structures of the clouds from MMR compare well with
310 the radar reflectivity from CloudSat by retrieving the high clouds around 47N° and
311 low clouds around 52N°. The PF experiment has difficulties in detecting the cloud
312 tops appropriately. PF tends to detect a large quantity of low clouds; by adding a set of
313 particles with small-fraction clouds in APF, higher clouds can be reproduced, which is
314 consistent with the implications from Fig. 2b and 2d. APF detects clear strong cloud
315 signals and removes the cloud fractions on near-surface levels around 36 N°
316 successfully. Since the existences of ground-layer radar reflectivity are likely
317 corresponding to the strong reflection from the underlying surface of the earth, the
318 height of cloud bases of MMR and PF are not compared in this sub-section. The
319 experiments with larger size of particles including 0% to 20% (at the interval of 1%)
320 plus 30% to 100% (at the interval of 10%) or of 0% to 100% (at the interval of 1%)
321 one-layer cloud profiles (introduced in section 2) yield similar results from APF but
322 are much more costly (not shown).

323

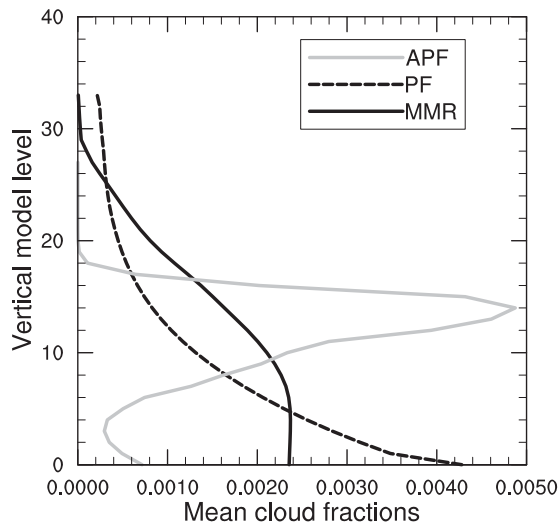


324

325 **Figure 3.** (a) The radar reflectivity (units: DBZ) cross sections from CloudSat, (b) the MMR
 326 retrieved cloud fractions (units: %) cross sections, (c) the PF retrieved cloud fractions, and (d) the
 327 APF retrieved cloud fractions valid at 1100 UTC 3 June 2012.

328 The vertical profiles of the averaged cloud fractions from MMR, PF, and APF are
 329 plotted in Fig. 4 at 1100 UTC 3 June 2012 with AIRS. Both MMR and PF
 330 experiments yield ambiguous cloud distributions, whereas APF retrieves much
 331 stronger cloud signals constrained between level-2 to level-20 (approximately from
 332 950hPa to 400hPa). More clouds around level 10 are retrieved (approximately 750hPa)
 333 in MMR, while PF is prone to retrieving clouds near surface levels. Note that MMR
 334 retrieves much higher cloud tops and lower cloud bases compared to APF. The cloud
 335 base from PF is lowest; the cloud top from MMR and PF is comparable. Only the
 336 APF related methods will be further discussed in later sections owing to the missing
 337 of high clouds using PF.

338



339
340 **Figure 4.** The mean cloud fraction on all model levels for the experiments MMR, PF, and APF

341 with AIRS observations valid at 1100 UTC 3 June 2012.

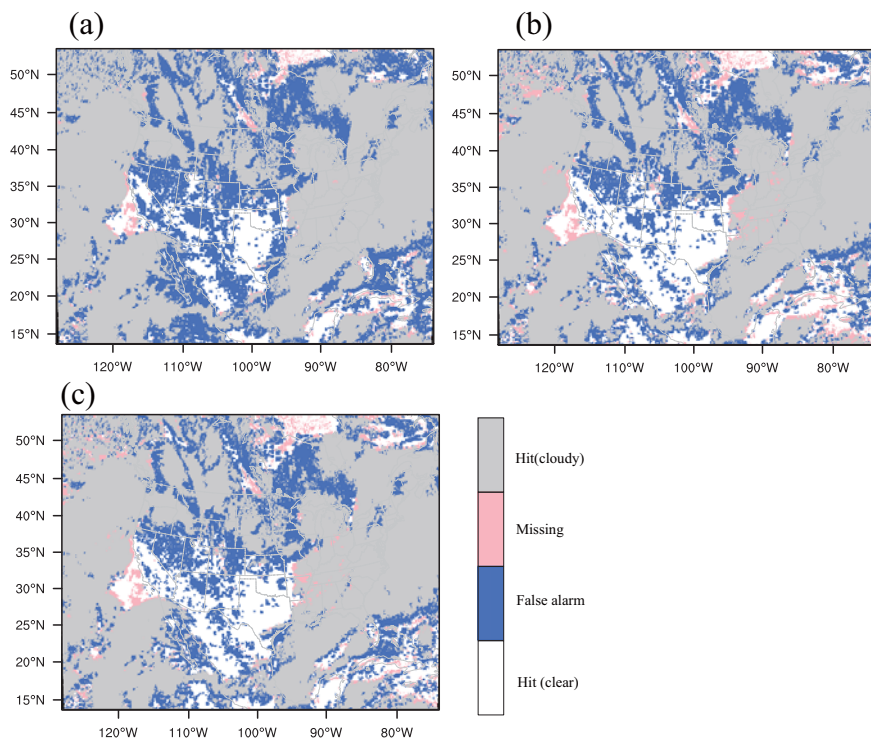
anna 2016-08-06 08:35 ✓
删除的内容: from

342 4.3 Cloud mask

343 Comparison experiments on real cases are further performed for over longer time
344 period from 0000 UTC 12 December 2013 to 0700 UTC 12 December 2013. The
345 cloud mask is marked as cloudy when there is a recognizable existence of cloud on
346 any level from MMR or PF retrievals. Both the NASA GOES Imager products and the
347 MMR-retrieved fields are interpolated to the same $0.1^{\circ} \times 0.1^{\circ}$ latitude–longitude grid
348 with 0 for clear and 1 for cloudy before the comparisons for verification. Fig. 5 shows
349 the *hits*, *false_alarms* and *misses* locations with the use of GOES-Imager, MODIS,
350 CrIS, AIRS, and IASI radiances in the retrieval algorithms at 0700 UTC 12 December
351 2013. Note that, cloud mask retrievals from both the MMR and APF hit the clear and
352 cloudy events well in Fig. 5a and 5b. In most areas, the MMR experiment

anna 2016-08-06 08:39 ✓
删除的内容: radiances from

353 overestimated the cloud mask with more false alarm events compared to the APF
 354 experiment, since the MMR solution is an “overly smoothed” estimation of the true
 355 vertical profile. It seems that the accuracy of cloud detection is lower for areas with
 356 high altitude than under tropical conditions, indicating that the smaller lapse rate in
 357 the atmosphere will lead radiance less sensitivity to clouds over polar areas. Fig. 5c
 358 shows the cloud mask results from the APFg2 experiment without the perturbed
 359 particles in group-1 introduced in section 2. There is no large discrepancy between
 360 Fig. 5b and Fig. 5c, suggesting that the particles in group-2 that fully span the
 361 possibility of the cloud distributions, are more determinant in retrieving the cloud
 362 mask.
 363



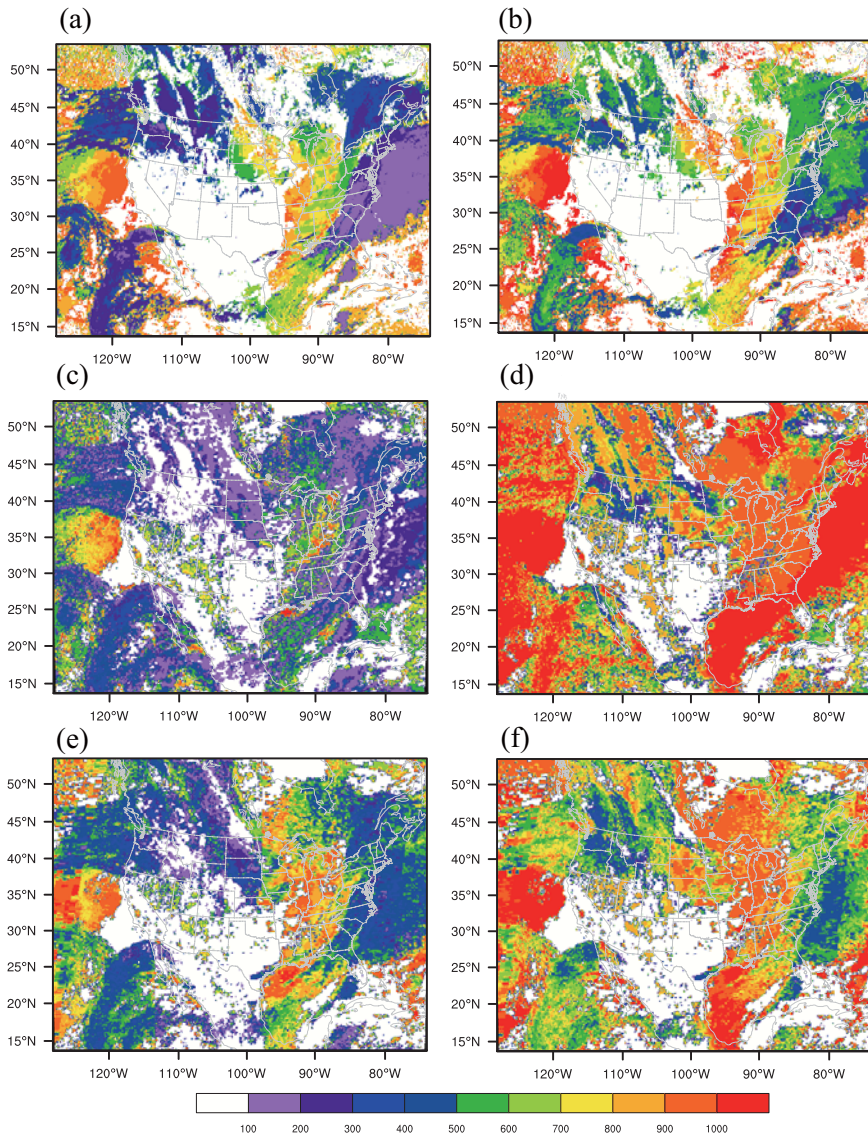
364

365 **Figure 5.** The false alarms, misses, and hits for clear and cloudy event locations with (a) the MMR
366 method, (b) the APF method, and (c) the APF method but without the group-1 particles (see text
367 for detailed explanations) valid at 0700 UTC 15 December 2013.

368 4.4 Cloud top and base pressure

369 The retrieved cloud top pressures (CTP) and cloud bottom pressures (CBP) from
370 this study along with the NASA GOES cloud products are illustrated in Fig. 6. The
371 CTPs from both methods are in good accordance with the NASA cloud products for
372 high clouds (from 100 hPa to 600 hPa) in Fig. 6a, 6c, and 6e. The retrieved cloud top
373 heights from MMR are overall higher than those from the NASA reference, especially
374 for lower clouds at approximately 750-1000 hPa (e. g., between longitude -100° and
375 -90°). On the other hand, the CTPs from APF are much closer to those in the
376 reference for both high and low clouds. APF overestimates the CBPs for some low
377 clouds (putting the clouds too low) in Fig. 6f; the overestimation of the CBP is even
378 more obvious from MMR in most regions in Fig. 6d.

379



380

381 **Figure 6.** The cloud top pressure (left panels) from (a) the NASA GOES retrieval, (c) the MMR

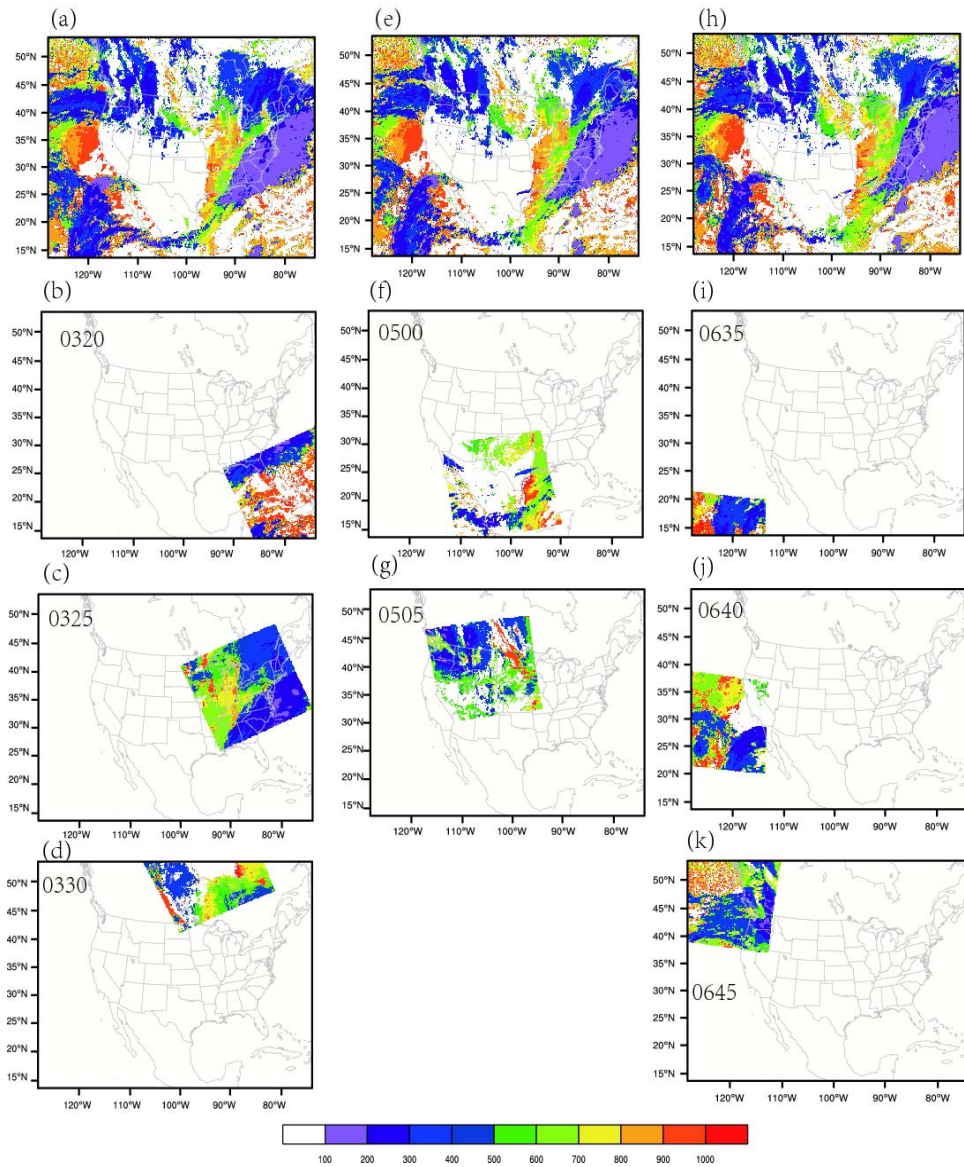
382 method, (e) the APF method, and the cloud bottom pressure (right panels) from (b) the NASA

383 GOES retrieval, (d) the MMR method, (f) the APF method valid at 0700 UTC 15 December 2013.

384 The CTPs from NASA GOES cloud products for more hours (0300UTC,

385 0500UTC, 0700UTC) together with the independent CTP retrievals from MODIS

386 level-2 products (http://modis-atmos.gsfc.nasa.gov/MOD06_L2/) are plotted in Fig. 7.
387 Different sub-periods of the MODIS cloud retrieval products (e.g., Fig. 7b valid at
388 0320 UTC, Fig. 7c at 0325, and Fig. 7d at 0330 UTC) are chosen to approach the
389 valid times in Fig. 7a, Fig. 7e, and Fig. 7h respectively. The CTPs from both cloud
390 products agree well for both high and low clouds, confirming that NASA GOES cloud
391 products are overall reliable for verifying the cloud retrievals and MODIS level-2
392 products can also be applied for validations.



393

394 **Figure 7.** The cloud top pressure for (a) 0300UTC from the GOES NASA retrieval, (b) 0320UTC,

395 (c) 0325UTC, (d) 0330UTC from MODIS level-2 products; (e) 0500UTC from the GOES NASA

396 retrieval, (f) 0500UTC, (g) 0505UTC; (h) 0700UTC from the GOES NASA retrieval, (i)

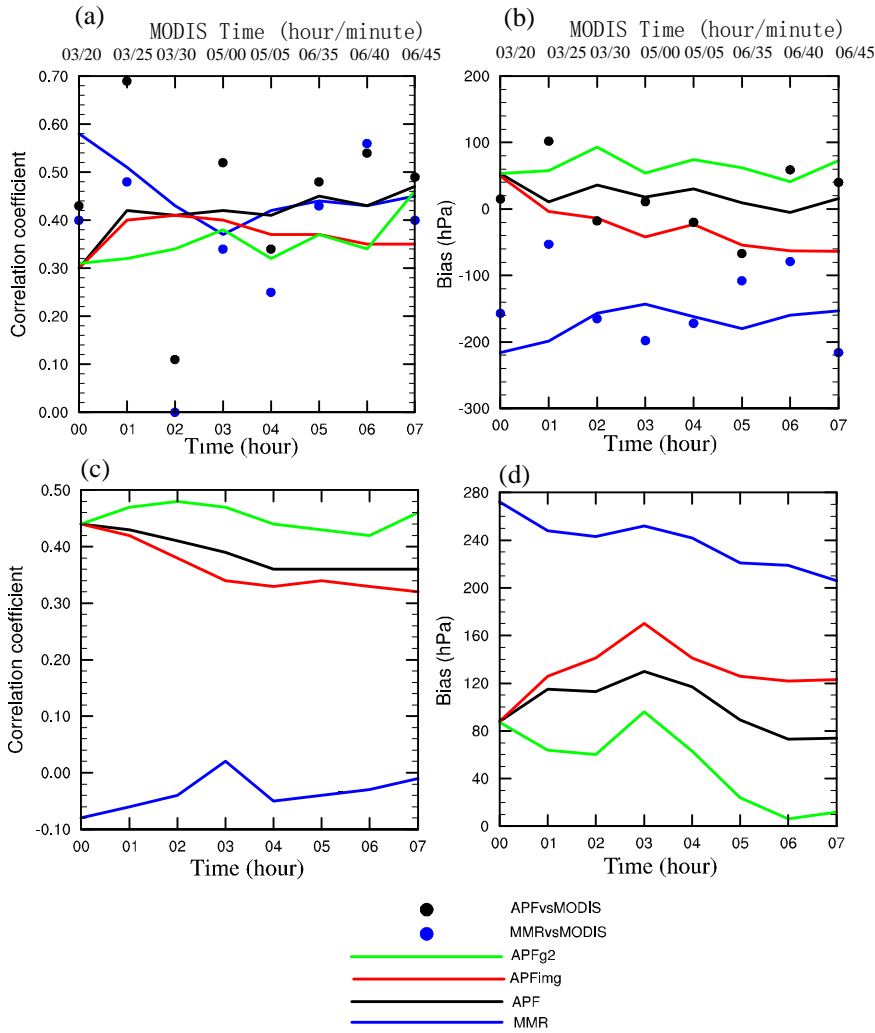
397 0635UTC, (j) 0640UTC, and (k) 0645UTC from MODIS level-2 products.

398 Fig. 8 presents the correlation coefficients and biases of the CTP and CBP verified
399 against the NASA GOES and MODIS retrievals. The solid lines denote the results
400 regarding the CTP and CBP versus the NASA GOES products from 0000 UTC to
401 0700 UTC, while the dots describe the CTP results versus the cloud top retrievals in
402 NASA MODIS level-2 products at 0320UTC, 0325UTC, 0330UTC, 0500UTC,
403 0505UTC, 0635UTC, 0640UTC, and 0645UTC. Here the negative bias means that the
404 retrieved clouds are higher than the reference. Vice versa, the positive bias indicates
405 the clouds are put too low. We conducted another experiment “APFing” that applies
406 solely GOES Imager data to check the added value from the high spectral resolution
407 radiances (such as, CrIS, AIRS, and IASI). In Fig. 8a, the correlations between the
408 retrievals from MMR and the NASA GOES retrievals are comparable with from APF
409 for most hours; APF gains overall higher correlations with the CTPs in the MODIS
410 retrievals. From the bias in Fig. 8b, it seems that the CTPs from MMR are
411 underestimated (putting the clouds too high) consistently against both retrievals with
412 GOES and MODIS radiances. Fig. 8c shows that the correlations are weaker for
413 MMR compared to others all the time. In Fig. 8d, the positive CBP biases from MMR
414 are remarkable, while the CBP biases from APF are largely reduced. Generally,
415 APFing degrades the CTP and CBP results consistently, suggesting that radiances
416 with high spectral resolutions are able to improve the vertical descriptions of cloud
417 profiles. It is found that the clouds retrieved with APFg2 are shrunken in terms of
418 cloud depth with notably lower cloud top and higher cloud base compared to APF,
419 when excluding the perturbed particles in the first group.

anna 2016-08-06 08:40



删除的内容: from



421

422 **Figure 8.** (a) Correlation coefficient, (b) bias for the cloud top pressure, (c) correlation coefficient,

423 and (d) bias for the cloud bottom pressure versus the NASA GOES retrievals from 0600 UTC 15

424 December 2013 to 0700 UTC 15 December 2013. Black and blue dots denote results versus the

425 MODIS level-2 cloud top pressure retrieval valid at 0320UTC, 0325UTC, 0330UTC, 0500UTC,

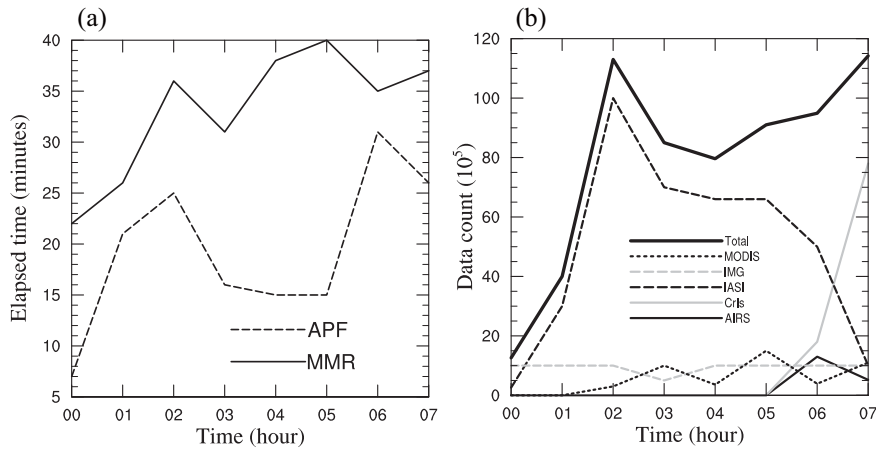
426 0505UTC, 0635UTC, 0640UTC, and 0645UTC. The valid times for the MODIS level-2 data are

删除的内容:

427 shown on the top of the x-axis.

428 4.5 Computational issues

429 Fig. 9a represents the elapsed times for the MMR and APF experiments and the
430 counts of radiance observations in use are shown in Fig.9b from 0000 UTC to 0700
431 UTC 12 December 2013. The profile of computing time in MMR is quite different
432 from that in PF. The cost of MMR is dominated by the heavy minimization procedure,
433 while APF is more associated with the processes of initializing particles and
434 calculating weights for all the particles. The computing times were measured from
435 cloud retrieving runs with 64 MPI-tasks on a single computing node in an IBM
436 iDataPlex Cluster. The measured wall clock computing times show that generally
437 MMR is computationally more expensive for most of the time than APF. It seems the
438 wall clock times for MMR are generally proportional to the data amount used. While
439 for the APF experiment, the wall clock time is mostly determined by the particles size
440 and partly affected by the channel number, such as for 2013121202 and 2013121206,
441 when the total counts of the hyperspectral sensors (IASI, CrIs, and AIRS) are large.
442 The PF experiments using particles of one-layer cloud with 100% cloud fractions
443 usually take less than 5 minutes for the same periods (not shown).



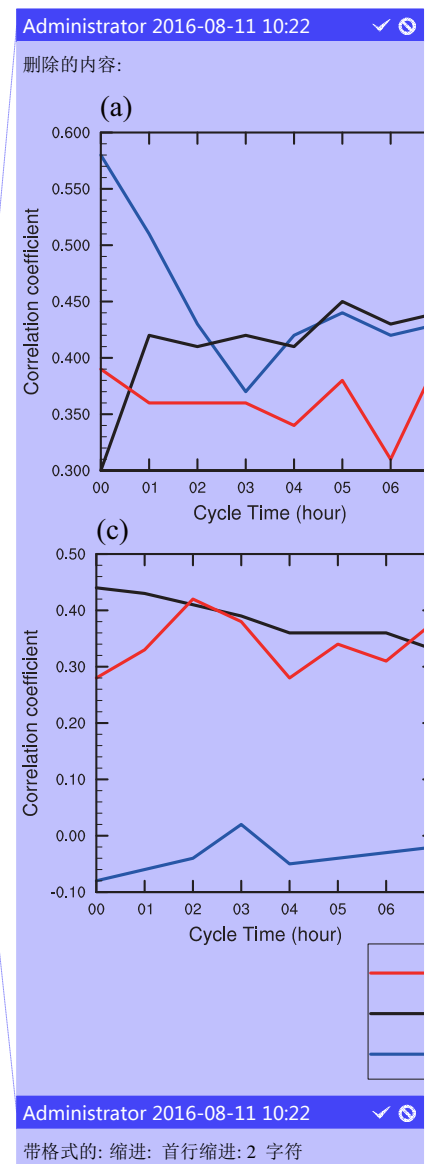
444
 445 **Figure 9.** (a) The elapsed time and (b) the data count from 0000 UTC to 0700 UTC 15 December
 446 2013.

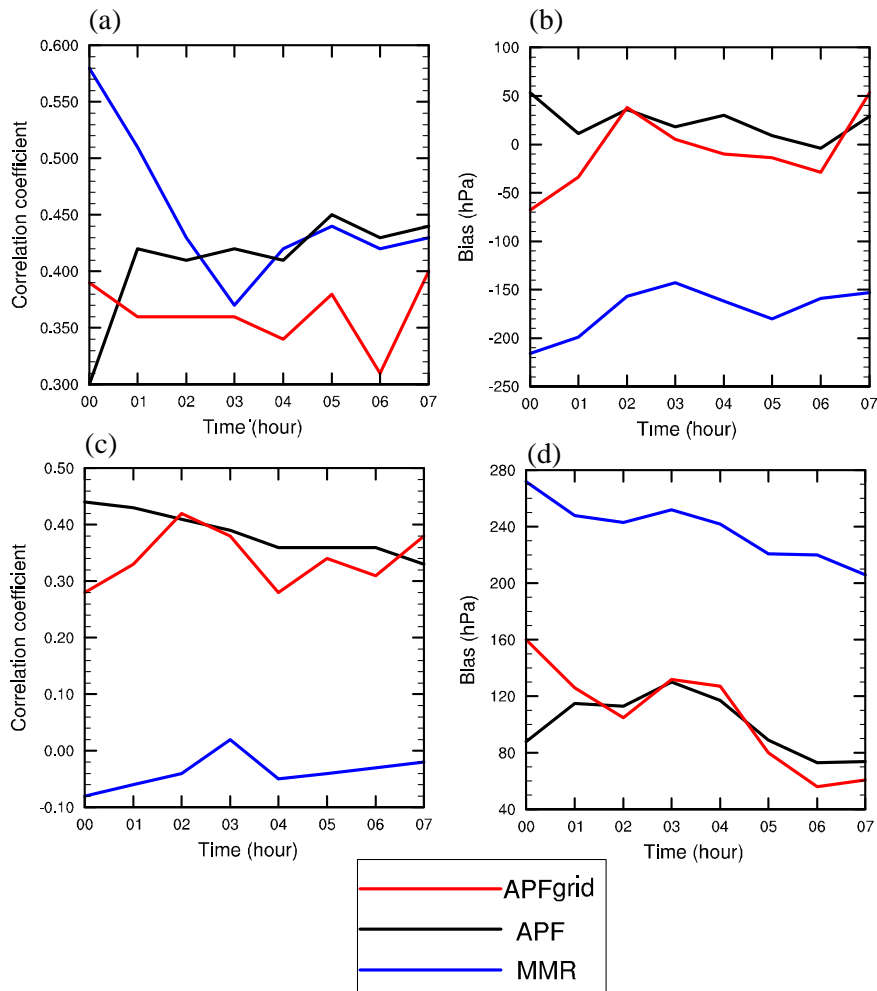
447 4.6 Resolving the filtering problem on model grids

448 As explained in subsection 3.3, the filtering problem is resolved in the radiance
 449 observational space at each FOV of each sensor independently and sequentially. For
 450 each FOV, the retrieved cloud fractions are extrapolated to its neighboring model grid
 451 points afterwards. We order the sensors in the cloud retrieving procedure as
 452 GOES-Imager, MODIS, CrIS, AIRS, and IASI, aiming to optimize the vertical clouds
 453 using sensors featured with sufficient spectral resolutions. As a consequence, the
 454 retrievals from the last sensor determine the final output to the most extent, causing
 455 the cloud retrievals highly subjective to the ordering of the sensors. On the other hand,
 456 it means the information from other prior sensors will be more or less discarded. In
 457 this section, a different way of resolving the filtering problem is preliminarily tested,
 458 in which the weights for each particle are aggregated over all available sensors by

459 calling the forward radiative transfer model on neighbouring model grids.

460 Fig. 10 shows the clouds retrievals from the grid-based method. It is noted that
461 the grid-based scheme yields slightly worse results of CTP and neutral results of CBP
462 compared with those from the observation-based (FOV-based) scheme, indicating that
463 the hyperspectral sensors probably favor the retrieved CTP and CBP in the
464 FOV-based scheme, which are available for most of the time. It is worth pointing out
465 that the ordering of different sensors has nearly no effect on the final cloud retrievals,
466 when the weights of the particles are calculated in model space (not shown). The final
467 cloud retrieval is no longer overwritten by the retrieval from the last sensor but is a
468 total solution with all the sensors fairly considered, instead. The computational cost of
469 retrieving clouds in model space is comparable or slightly heavier than that in
470 observation space. The computational cost of the grid-based scheme scales with the
471 number of the computing nodes more directly, compared to that of the FOV-based
472 scheme.





473

474 **Figure 10.** (a) Correlation coefficient, (b) bias for the cloud top pressure, (c) correlation

475 coefficient, and (d) bias for the cloud bottom pressure versus the NASA GOES retrievals from

476 0000 UTC to 0700 UTC 15 December 2013.

477 **5. Discussion and conclusion**

478 This study presents a new cloud retrieval method based on the particle filter (PF)
479 in the framework of GSI, as a competitive alternative to the MMR method. The
480 behaviors of different particle initializations are demonstrated on one single field of
481 view and the CONUS domain respectively. Comparisons between the PF and the
482 MMR method are conducted in terms of the features of cloud mask, cloud top, cloud
483 base, and the vertical distributions of clouds. It was found that the PF method
484 retrieves clear cloud signals while MMR is more ambiguous in detecting clouds. By
485 adding more small-fraction particles, high clouds can be better interpreted. From the
486 statistical results, it was found that MMR underestimates the cloud top pressures (put
487 the clouds top too high) and overestimates the cloud bottom pressures (put the clouds
488 top too low) as well. APF improves both the retrievals of cloud tops and cloud bases
489 remarkably, especially for the cloud bases. As expected, radiances with high spectral
490 resolutions contribute to quantitative cloud top and cloud base retrievals. In addition,
491 a different way of resolving the filtering problem over each model grid is tested to
492 aggregate the weights with all available sensors considered, which is proven to be less
493 constrained by the ordering of sensors. Last but not least, the PF method is overall
494 more computationally efficient; the cost of the model grid-based PF method scales
495 more directly with the number of the computing nodes.

496 In future work, validation studies using multispectral imagers on geostationary
497 satellites, spaceborne lidars (or radar), and surface site data will continue, and the
498 results will be used to update the retrieval algorithm. Maximizing the consistency in
499 the products across platforms and optimizing the synergistic use of multiple-source

500 radiances in the new algorithm are important aspects. To estimate the flow dependent
501 uncertainties in the cloud analysis and in the forecasts, the ensemble nowcasting with
502 three dimensional cloud fractions via the rapid-update cycling mode is also planned.
503 Increasing the highest extent cloudy cases will be included in future studies. Finally,
504 the use of cloud liquid water and ice mixing ratios retrieved from the cloud fractions
505 using multi-sensor radiances to pre-process the first guess in numerical weather
506 forecast is another promising application.

507 **Code and/or data availability**

508 The MMR cloud retrieval codes can be obtained freely from
509 (<http://www2.mmm.ucar.edu/wrf/users/wrfda/>). The other codes can be obtained by
510 emails from the authors.

511 **Acknowledgments**

512 This work was jointly sponsored by the Natural Science Foundation of Jiangsu
513 Province under Grant No BK20160954, the 973 Program (Grant No. 2013CB430102)
514 , the Beijige Funding from Jiangsu Research Institute of Meteorological Science
515 (BJG201510), the National Natural Science Foundation of China (41375025), and the
516 Priority Academic Program Development of Jiangsu Higher Education Institutions
517 (PAPD). The authors would like to thank Chris Davis for fruitful discussions, and to
518 Bobbie Weaver for editing the manuscript. We greatly thank the anonymous reviewers
519 for their valuable comments on the earlier versions of the manuscript.

520 **REFERENCES**

- 521 Ackerman, S. A., K. I. Strabala, W. P. Menzel, R. A. Frey, C. C. Moeller, and L. E.
522 Gumley: Discriminating clear sky from clouds with MODIS, *Geophys. Res.*
523 *Atmos.*, 103, 32141-32157, 1998.
- 524 Auligné, T., Lorenc, A., Michel, Y., Montmerle, T., Jones, A., Hu, M., and Dudhia, J.:
525 Toward a New Cloud Analysis and Prediction System, *B Am Meteorol Soc*, 92,
526 207-210, 2011.
- 527 Auligné, T.: Multivariate minimum residual method for cloud retrieval. Part I:
528 Theoretical aspects and simulated observation experiments, *Monthly Weather*
529 *Review*, 142, 4383-4398, 2014a.
- 530 Auligné, T.: Multivariate minimum residual method for cloud retrieval. Part II: Real
531 observations experiments, *Monthly Weather Review*, 142, 4399-4415, 2014b.
- 532 Aumann, H. H., Chahine, M. T., Gautier, C., Goldberg, M. D., Kalnay, E., McMillin,
533 L. M., Revercomb, H., Rosenkranz, P. W., Smith, W. L., and Staelin, D. H.:
534 AIRS/AMSU/HSB on the Aqua mission: Design, science objectives, data products,
535 and processing systems, *Geoscience and Remote Sensing, IEEE Transactions on*,
536 41, 253-264, 2003.
- 537 Bayler, G. M., Aune, R., and Raymond, W.: NWP cloud initialization using GOES
538 sounder data and improved modeling of nonprecipitating clouds, *Monthly weather*
539 *review*, 128, 3911-3920, 2000.
- 540 Berrocal, V. J., Raftery, A. E., and Gneiting, T.: Combining spatial statistical and
541 ensemble information in probabilistic weather forecasts, *Monthly Weather Review*,
542 135, 1386-1402, 2007.
- 543 Blumstein, D., Chalon, G., Carlier, T., Buil, C., Hebert, P., Maciaszek, T., Ponce, G.,
544 Phulpin, T., Tournier, B., and Simeoni, D.: IASI instrument: Technical overview
545 and measured performances, *Optical Science and Technology, the SPIE 49th*
546 *Annual Meeting*, 2004, 196-207,
- 547 Brückner, M., Pospichal, B., Macke, A., and Wendisch, M.: A new multispectral cloud
548 retrieval method for ship - based solar transmissivity measurements, *Journal of*
549 *Geophysical Research: Atmospheres*, 119, 2014.
- 550 Descombes, G., Auligne, T., and Lin, H.-C., Xu, D., Schwartz, C. S., Vandenberghe, F.:
551 Multi-sensor Advection Diffusion nowCast (MADCast) for cloud analysis and
552 short-term prediction., *NCAR Technical Note NCAR/TN-509+STR*, , 21 pp.,
553 2014.
- 554 Eyre, J. R., and Menzel, W. P.: Retrieval of cloud parameters from satellite sounder
555 data: A simulation study, *Journal of Applied Meteorology*, 28, 267-275, 1989.
- 556 Han, Y., Delst, P. V., Liu, Q., Weng, F., Yan, B., Treadon, R., and Derber, J.: JCSDA
557 Community Radiative Transfer Model (CRTM)—Version 1, *NOAA Tech. Rep.*
558 *NESDIS*, 122, 33, 2006.
- 559 Hu, M., Xue, M., and Brewster, K.: 3DVAR and Cloud Analysis with WSR-88D
560 Level-II Data for the Prediction of the Fort Worth, Texas, Tornadoic Thunderstorms.
561 Part I: Cloud Analysis and Its Impact, *Monthly Weather Review*, 134, 675-698,
562 10.1175/mwr3092.1, 2006.
- 563 Huang, H.-L., Smith, W. L., Li, J., Antonelli, P., Wu, X., Knuteson, R. O., Huang, B.,

564 and Osborne, B. J.: Minimum local emissivity variance retrieval of cloud altitude
565 and effective spectral emissivity-simulation and initial verification, *Journal of*
566 *applied meteorology*, 43, 795-809, 2004.

567 Karlsson, K.-G., Johansson, E., and Devasthale, A.: Advancing the uncertainty
568 characterisation of cloud masking in passive satellite imagery: Probabilistic
569 formulations for NOAA AVHRR data, *Remote Sensing of Environment*, 158,
570 126-139, 2015.

571 Kleist, D. T., Parrish, D. F., Derber, J. C., Treadon, R., Wu, W. S., and Lord, S.:
572 Introduction of the GSI into the NCEP Global Data Assimilation System, *Weather*
573 *and Forecasting*, 24, 1691-1705, 10.1175/2009waf2222201.1, 2009.

574 Liu, Q., and Weng, F.: Advanced doubling-adding method for radiative transfer in
575 planetary atmospheres, *Journal of the atmospheric sciences*, 63, 3459-3465, 2006.

576 Mace, G. G., 2004: Level 2 GEOPROF product process description and interface
577 control document (v.3): Level 2 GEOPROF product process description and
578 interface control document (v.3), Tech. rep., CIRA, Colorado State University,
579 2004.

580 Mechri, R., Ottlé, C., Pannekoucke, O., and Kallel, A.: Genetic particle filter
581 application to land surface temperature downscaling, *Journal of Geophysical*
582 *Research: Atmospheres*, 119, 2131-2146, 2014.

583 Menzel, W., Smith, W., and Stewart, T.: Improved cloud motion wind vector and
584 altitude assignment using VAS, *Journal of Climate and Applied meteorology*, 22,
585 377-384, 1983.

586 Menzel, W. P., and Purdom, J. F.: Introducing GOES-I: The first of a new generation
587 of geostationary operational environmental satellites, *B Am Meteorol Soc*, 75,
588 757-781, 1994.

589 Platnick, S., King, M. D., Ackerman, S. A., Menzel, W. P., Baum, B. A., Riédi, J. C.,
590 and Frey, R. A.: The MODIS cloud products: Algorithms and examples from Terra,
591 *Geoscience and Remote Sensing, IEEE Transactions on*, 41, 459-473, 2003.

592 Rossow, W. B., and Schiffer, R. A.: ISCCP cloud data products, *B Am Meteorol Soc*,
593 72, 2-20, 1991.

594 Rossow, W. B., Walker, A. W., and Garder, L. C.: Comparison of ISCCP and other
595 cloud amounts, *Journal of Climate*, 6, 2394-2418, 1993.

596 Shen, Z. Q., and Tang, Y. M.: A modified ensemble Kalman particle filter for
597 non-Gaussian systems with nonlinear measurement functions, *J Adv Model Earth*
598 *Sy*, 7, 50-66, 2015.

599 Skamarock, W., C, Klemp, J. B., Dudhia, J., Gill, D. O., Barker, D. M., Duda, G.,
600 Huang, X.-Y., Wang, W., and Powers, J. G.: A description of the Advanced
601 Research WRF version 3., NCAR, 113, 2008.

602 Smith, A., Atkinson, N., Bell, W., and Doherty, A.: An initial assessment of
603 observations from the Suomi - NPP satellite: data from the Cross - track Infrared
604 Sounder (CrIS), *Atmospheric Science Letters*, 16, 260-266, 2015.

605 Snyder, C., and Zhang, F. Q.: Assimilation of simulated Doppler radar observations
606 with an ensemble Kalman filter, *Monthly Weather Review*, 131, 1663-1677, Doi
607 10.1175//2555.1, 2003.

608 Stephens, G. L., Vane, D. G., Boain, R. J., Mace, G. G., Sassen, K., Wang, Z.,
609 Illingworth, A. J., O'Connor, E. J., Rossow, W. B., and Durden, S. L.: The
610 CloudSat mission and the A-Train: A new dimension of space-based observations
611 of clouds and precipitation, *B Am Meteorol Soc*, 83, 1771-1790, 2002.
612 van Leeuwen, P. J.: Nonlinear data assimilation in geosciences: an extremely efficient
613 particle filter, *Quarterly Journal of the Royal Meteorological Society*, 136,
614 1991-1999, 2010.
615 Wu, W.-S., Purser, R. J., and Parrish, D. F.: Three-dimensional variational analysis
616 with spatially inhomogeneous covariances, *Monthly Weather Review*, 130,
617 2905-2916, 2002.
618 Wu, X., and Smith, W. L.: Assimilation of ERBE data with a nonlinear programming
619 technique to improve cloud-cover diagnostics, 120, 2009-2004, 1992.
620 Xu, D., Auligné, T., and Huang, X.-Y.: A Retrieval Method for 3-D Cloud Parameters
621 Using Radiance Observations from Multiple Satellites, *Advances in atmospheric*
622 *physics*, 32, 349-362, 2015.
623 Xu, D. M., Liu, Z. Q., Huang, X. Y., Min, J. Z., and Wang, H. L.: Impact of
624 assimilating IASI radiance observations on forecasts of two tropical cyclones,
625 *Meteorology and Atmospheric Physics*, 122, 1-18, 10.1007/s00703-013-0276-2,
626 2013.
627 Zhao, C., Xie, S., Klein, S. A., Protat, A., Shupe, M. D., McFarlane, S. A., Comstock,
628 J. M., Delanoë, J., Deng, M., and Dunn, M.: Toward understanding of differences
629 in current cloud retrievals of ARM ground - based measurements, *Journal of*
630 *Geophysical Research: Atmospheres*, 117, 2012.
631

632